TECTONICS, VOL. 13, NO. 5, PAGES 1093-1107, OCTOBER 1994

Mechanics of back arc deformation in Costa Rica: Evidence from an aftershock study of the April 22, 1991, Valle de la Estrella, Costa Rica, earthquake (M_W=7.7)

Marino Protti
Observatorio Vulcanológico y Sismológico de Costa Rica, Universidad Nacional, Heredia, Costa Rica

Susan Y. Schwartz
Institute of Tectonics and Earth Sciences Department, University of California, Santa Cruz

Abstract. The April 22, 1991, M_W=7.7 Valle de la Estrella, Costa Rica, earthquake represents back arc thrusting of the Caribbean plate beneath the Panama block along the North Panama Thrust Belt. Large back arc thrusting events are quite rare, occurring in only two other locations along the Sunda Arc and Japan Sea. To better understand the mechanics of back arc thrusting, we constrain the faulting geometry associated with the 1991 Costa Rica earthquake using aftershock locations and focal mechanisms obtained from a three-component portable digital network deployed in and around the aftershock area following the mainshock. The spatial distribution of aftershocks reveals a complicated faulting geometry in the rupture area. Focal mechanisms determined from inversion of *P* wave and tangentially and radially polarized S wave (SH and SV, respectively) amplitudes recorded by this temporary network confirm fault complexity and indicate active thrust, normal and strike-slip faults in the back arc of Costa Rica. Most of the thrust events are confined to the southern portion of the aftershock zone in the vicinity of the mainshock. Their distribution suggests the existence of a near-horizontal basal fault plane at a depth of about 15 km, with many imbricate faults having steeper dips extending from the basal plane toward the surface. Events with strike-slip mechanisms locate northwest of the thrust events and define a SW-NE trending, left-lateral strike-slip fault zone that represents the NW termination of the mainshock rupture and possibly the maximum NW extension of the Panama block. The superposition of the aftershock locations on a geologic map of the region shows that aftershocks are restricted to occur in the older, more competent rock units (volcanic and volcaniclastic rocks interbedded with carbonates) of the back arc sedimentary basin. Shallow events (*depth*<5 km) occur only where these oldest units are exposed at the surface. This suggests that (1) exposure of the lower units results from repeated earthquake slip on the shallow crustal faults imaged by the aftershocks and (2) as much as 7 km of basin fill material, overlying the lower units, northeast of the mainshock, does not deform seismically but, instead, folds and possibly faults aseismically.

Paper number 94TC01319.
0278-7407/94/94TC-01319$10.00

Introduction

On April 22, 1991, at 2156:51.7 UTC a large earthquake (M_W=7.7) occurred in southeast Costa Rica, near Valle de la Estrella (Figure 1). This event produced extensive damage in Costa Rica, including 48 fatalities, 561 injuries, and 6841 homeless; similar damage occurred in Panamanian towns near the Costa Rica border [*Güendel et al.*, 1991].

Costa Rica is located on the western margin of the Caribbean plate (Figure 1). There the Cocos plate subducts under the Caribbean plate along the Middle America Trench at a rate of between 70 and 95 mm/y from Guatemala to southern Costa Rica, respectively (computed from [*DeMets et al.*, 1990]). It is along this plate boundary, at the western margin of Costa Rica, where most of the recent, large, destructive earthquakes have occurred (Figure 1). Southeast of Costa Rica is the Panama block. The northern boundary of the Panama block with the Caribbean plate is a convergent margin, the Panama Thrust Belt, that extends from the Caribbean coast of Colombia to south of Limón, Costa Rica [*Silver et al.*, 1990]. Inland within Costa Rica, this convergence has deformed the thick sediments of the Limón Basin. It was along this convergent plate boundary that the April 22, 1991, Valle de la Estrella earthquake occurred, thrusting the Caribbean plate beneath the Panama block along the northeast flank of the Talamanca Cordillera (Figure 1).

The April 22, 1991, event is not the only instrumentally recorded earthquake to occur in this region. On January 7, 1953, a moderate magnitude earthquake (M_S<6.0) produced damage in Limón, and on April 24, 1916, an M_S=7.4 earthquake, followed 2 days later by an M_S=7.1 aftershock, rocked the southern Caribbean coast of Costa Rica and northwestern portions of Panama [*Güendel*, 1986]. Other historical earthquakes in 1798 and 1822 are believed to have occurred in this region [*Montero et al.*, 1991]. Large back arc thrusting earthquakes are uncommon, with the last clear example occurring in the Japan Sea in 1993. Thus occurrence of the April 22, 1991, Costa Rica earthquake affords the rare opportunity to study a back arc thrusting event and improve our understanding of seismic deformation in this tectonic environment.

The April 22 earthquake and its larger aftershocks were well recorded by a local, countrywide seismographic network operated jointly by the Observatorio Vulcanológico y Sismológico de Costa Rica, Universidad Nacional (OVSICORI-UNA) and the Charles F. Richter Seismological Laboratory at

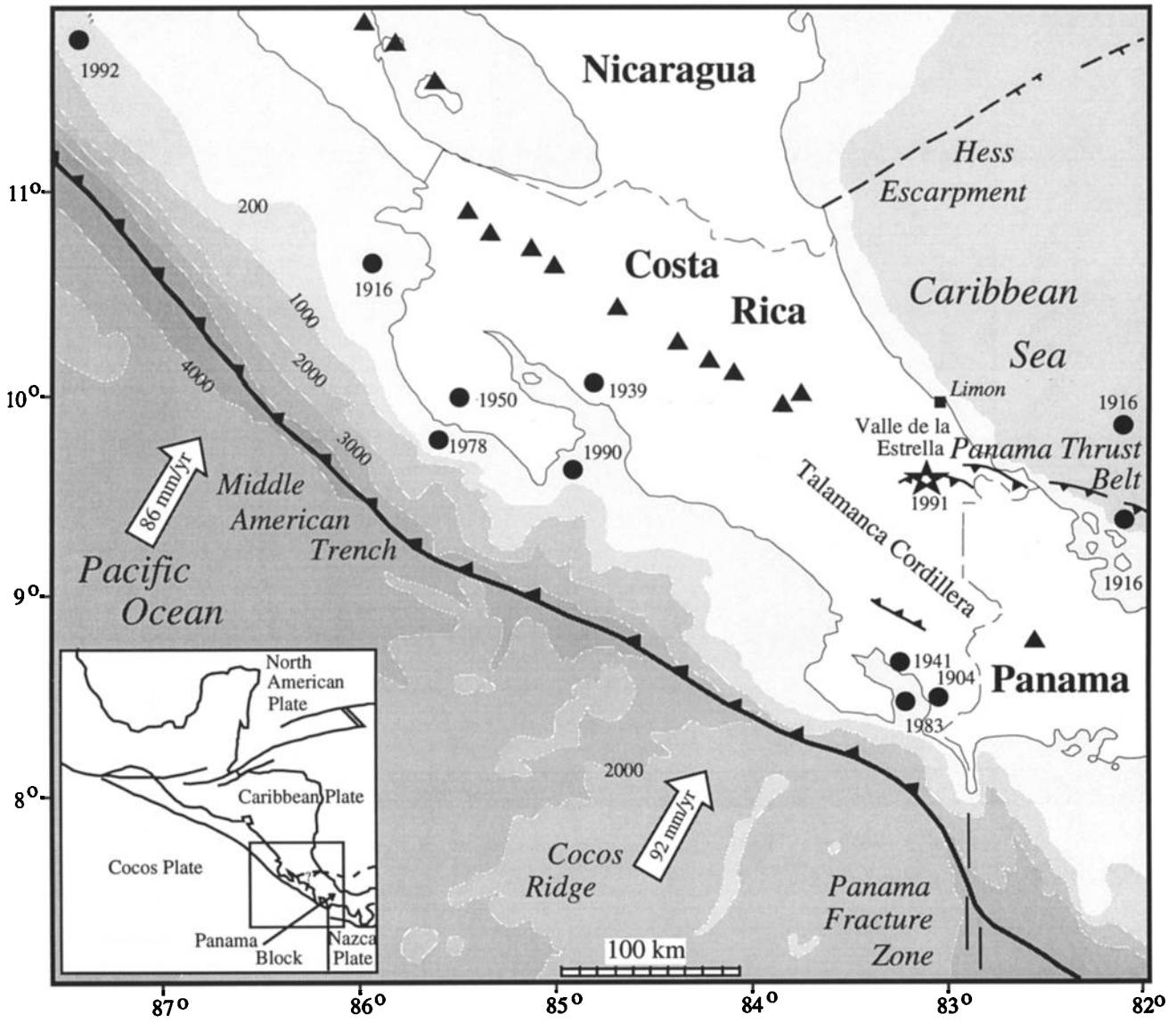

Figure 1. Tectonic setting of southern Central America and location of large ($M_S \geq 7.0$) earthquakes of this century (circles), including the April 22, 1991, Valle de la Estrella event (star). Triangles are active volcanoes. Convergence velocities between Cocos and Caribbean plates were computed using information from *DeMets et al.* [1990]. Bathymetric contours are in meters. Inset shows major plate boundaries in Central America and location of larger map.

the University of California, Santa Cruz. First motions from 22 local seismic stations in Costa Rica and Panama [*Montero et al.*, 1991], teleseismically recorded body and surface waves [*Goes et al.*, 1993], macroscopic crustal deformation [*Plafker and Ward*, 1992], leveling [*De Obaldía et al.*, 1991] and Global Positioning System (GPS) data [*Lundgren et al.*, 1993] all indicate a southeasterly striking fault plane dipping to the southwest. The dip determined using local first motions is significantly steeper (~40°) than that determined using teleseismic data (~15°). The geometry of this plane at depth and as it approaches the surface, i.e., whether it reaches the surface or dies out in the thick Cenozoic section blanketing the Caribbean plate-Panama block boundary, is not well understood.

Accurate locations have been determined for many of the larger aftershocks from data recorded by the local seismic network [*Montero et al.*, 1991]; however, the network's relatively large average station spacing precludes location of the smaller (M<3.0) aftershocks and thus a detailed picture of the mainshock faulting geometry. A temporary digital seismic network of five, three-component stations was deployed within and surrounding the rupture zone of the 1991 Valle de la Estrella earthquake [*Schwartz et al.*, 1991] to enhance station coverage and determine reliable locations of smaller aftershocks. This portable network (Figure 2) was deployed between May 8 and May 23, 1991, and recorded hundreds of small aftershocks, over 40 having magnitudes greater than 3.0. In this paper we use both aftershock locations and focal mechanisms to interpret the mode of deformation associated with this fascinating earthquake.

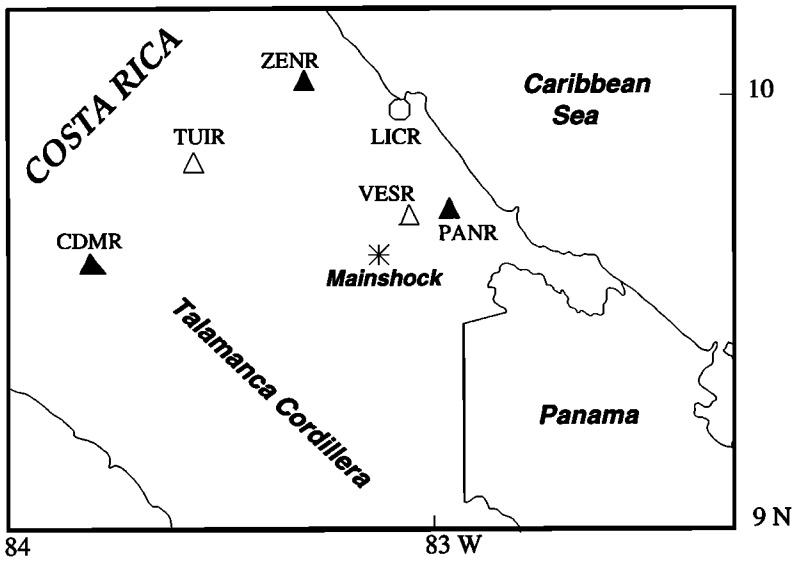

Figure 2. Location of the April 22, 1991, mainshock and stations used in our study. Solid triangles are stations with midperiod, three-component sensors; open symbols are stations with short-period, three-component (triangles) and vertical (circle) sensors.

Earthquake Locations

We used *P* and *S* wave arrival times from four stations of the portable digital network (CDMR, TUIR, VESR, and ZENR) and *P* wave arrival times from the closest permanent network station (LICR) (Figure 2) to locate aftershocks of the April 22, 1991, Costa Rica earthquake. Instrumentation at the portable stations consisted of Reftek 16-bit digitizers with short-period (2 Hz) sensors at stations TUIR and VESR and both short-period and midperiod (5 s) sensors at stations CDMR, ZENR, and PANR. Arrival times from station PANR were excluded from the location process owing to clock problems and near-station structural complexities that result in complicated waveforms that are difficult to interpret. Data profiles of the north component of ground motion for two aftershocks are shown in Figure 3. The waveforms are quite complicated, but initial arrival times are clear at all stations but PANR. At PANR, little energy arrives at the expected time of the *S* arrival (indicated by the diagonal, dashed line in Figure 3), with a large-amplitude arrival (possibly surface wave energy) following the expected *S* wave by over 2 s.

We picked *P* and *S* arrival times from the vertical and horizontal components, respectively, for nearly 400 events that were recorded at station LICR. From this group, 260 events with clear *P* and *S* arrivals at most of our digital stations were located. Reading errors are estimated to be <0.05 s for the digitally recorded *P* waves and ~0.1 s for the *S* waves and *P* waves read from paper records (station LICR).

Earthquakes are located using the program QUAKE3D [*Nelson and Vidale*, 1990] with a local two-dimensional velocity structure (Figure 4) that parallels the major geological and structural features of the region. This velocity model results from the combination and reinterpretation of (1) the velocity structure obtained by *Matumoto et al.* [1977] and used in routine earthquake location procedures in Costa Rica, (2) a shallow velocity structure for the Limón Basin provided by the Costa Rica Petroleum Refinery [*Montero et al.*, 1991], (3) the general trend of a velocity structure from a similar back arc environment in northern Honshu [*Zhao et al.*, 1992], and (4) offshore reflection data [*Astorga et al.*, 1991, J. Galewsky, personal communication, 1992].

The first step of the earthquake location procedure consists of computing travel times from every station to each node of a 20 x 100 x 50 km (1-km spacing), three-dimensional grid using the finite difference technique of *Vidale* [1990]. *S* wave travel times are obtained from *P* wave times assuming a constant Poisson ratio throughout the source volume. Tests to optimize the *P/S* velocity ratio (Figure 5) yield the lowest RMS residual for the earthquake population for a value of about 1.72. The second step uses the *P* and *S* wave travel time tables to obtain the temporal and spatial earthquake parameters by minimizing the residuals for a set of arrival times for each earthquake using an *L1* norm. Resolution in earthquake locations is higher than the node separation since travel times are interpolated between nodes. Duration magnitudes (*md*) were calculated for most events using a modified version of the magnitude equation employed by OVSICORI-UNA in their routine earthquake location procedure [*Protti Quesada et al.*, 1987].

Of our initial 260 earthquake locations we selected the best 107 events having eight or more arrival times (79 have nine arrivals, 5 *P* and 4 *S*) and RMS residuals <0.20 s for further consideration (Figure 6 and Table 1). In order to approximate the errors expected from our earthquake locations, we performed some synthetic experiments. The first test was designed to estimate location errors resulting from our rather sparse station coverage and realistic reading errors. Using the same receiver geometry as our data and the two-dimensional velocity model shown in Figure 4, we computed exact *P* and *S* wave arrival times for our best 107 events. We then added random time delays with an average amplitude determined from our estimated reading errors (-0.05 to 0.05 s for *P* arrivals and

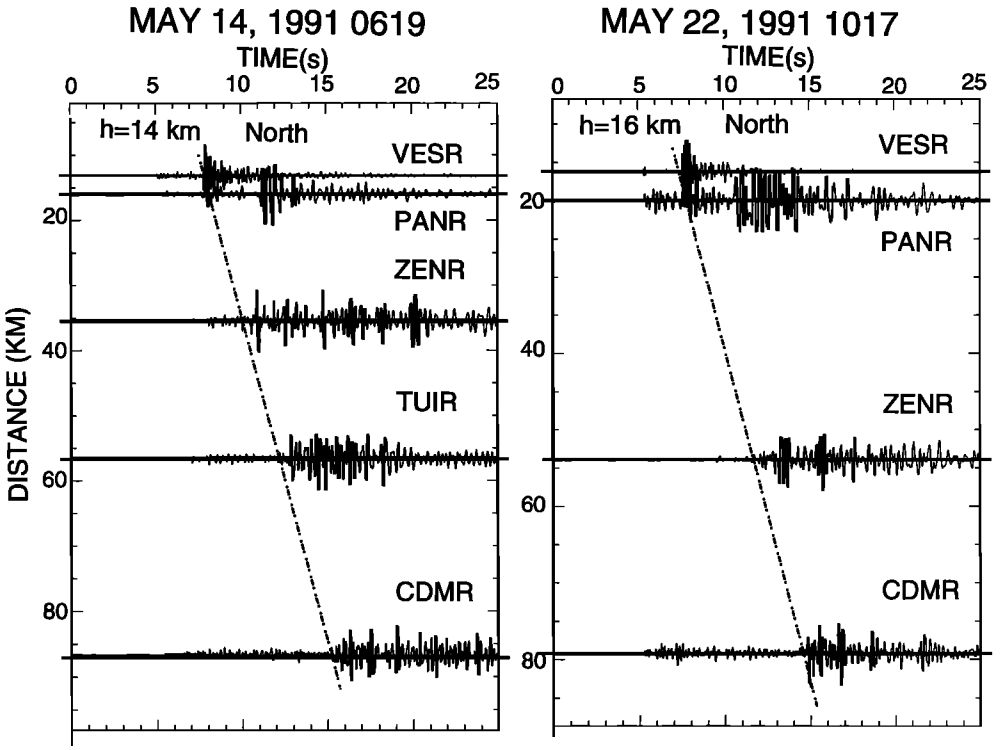

Figure 3. Data profiles of the north component of ground motion for two aftershocks. The dashed line marks the onset of the *S* wave arrival which is clear at all stations but PANR, where a large arrival is apparent over 2 s after the expected *S* onset. The event on May 22 is one of the 260 aftershocks we located but is not included in Table 1 since it does not satisfy our selection criteria.

-0.1 to 0.1 s for *S* arrivals) to the arrival time data. The average lengths of the horizontal and depth mislocation vectors obtained after the location procedure were 1.6 km and 2.3 km, respectively. Although these errors are fairly small, suggesting that relatively accurate earthquake locations can be obtained with our sparse station coverage, lack of exact knowledge of the crustal velocity structure will also contribute to errors in earthquake locations. To approximate more realistic errors to be expected in our aftershock locations, we repeated this test, locating the earthquakes in a velocity model perturbed from the one used to generate the arrival time data. Our perturbed velocity model was generated by adding Gaussian-distributed, random velocity perturbations with a mean of 5% over scale lengths of ~20 km to our original two-dimensional velocity structure. The inclusion of 5% random velocity perturbations to the original velocity model should

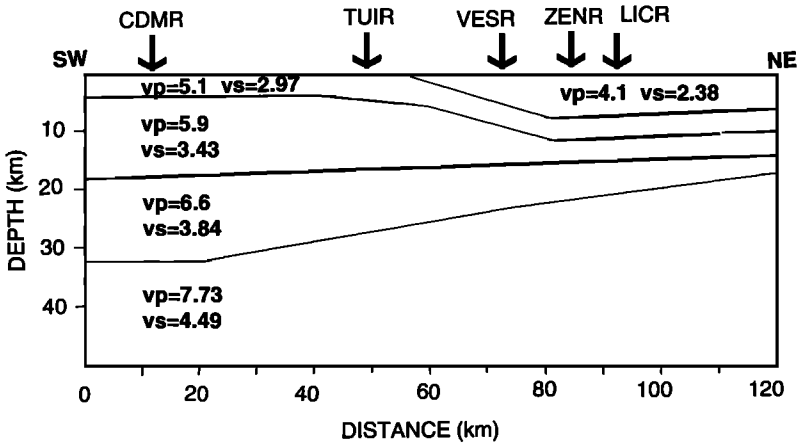

Figure 4. Two-dimensional velocity model used to determine aftershock locations. Arrows show the position of stations used for earthquake location. V_p and V_S are the velocities of *P* and *S* waves in km/s, respectively.

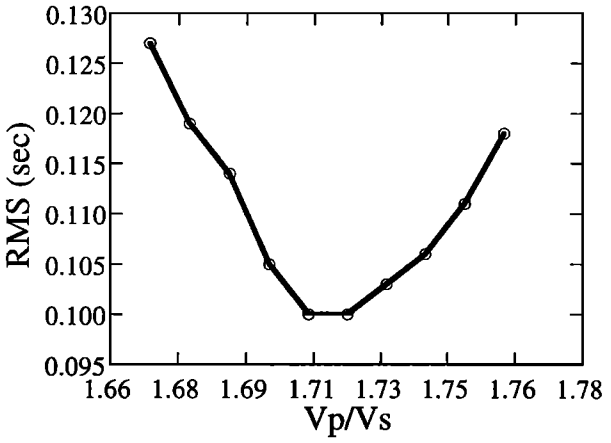

Figure 5. RMS residuals versus *Vp/Vs* ratios used to locate 260 aftershocks. This curve indicates that a *Vp/Vs* value of 1.72 yields the lowest residuals in the location procedure.

reflect realistic uncertainties in crustal velocities. The average lengths of the horizontal and depth mislocation vectors resulting from realistic uncertainties in both the velocity model and exact arrival times increase to 3.4 km and 3.6 km, respectively.

Focal Mechanism Determination

The classic method of using *P* wave first motions to obtain focal mechanism solutions from local network data is of limited use for most of our aftershock data since few seismic stations recorded clear first-motion observations and our estimated location errors may result in relatively large uncertainties in ray takeoff angles which are needed to calculate first-motion fault plane solutions. The amplitude of body waves (*P* and *S* waves) depends primarily on the seismic moment, orientation of the earthquake source, and station azimuth. Fault plane solutions calculated using amplitudes are less sensitive to source-receiver distance and earthquake focal depth than those determined from first motions. Body wave amplitudes have successfully been used by many workers to determine focal mechanisms from both teleseismically [*Pearce*, 1987] and locally recorded events [*Kisslinger*, 1980; *Slunga*, 1981; *Rognvaldsson and Slunga*, 1993]. We determine focal mechanisms for the larger Costa Rica aftershocks recorded at our temporary digital stations CDMR, TUIR, ZENR, and VESR through inversion of *P* wave and tangentially and radially polarized *S* wave (*SH* and *SV*, respectively) amplitudes using a grid-searching algorithm [*Schwartz*, 1993]. The inversion procedure consists of computing *P*, *SH* and *SV* reflectivity synthetics [*Wang and Herrmann*, 1980] for each source-station pair assuming all possible values for strike (0-360°), dip (0-90°), and rake (-180-180°) at 5° intervals, using the simple two-layered crustal velocity model of *Fan et al.* [1993], and determining the best focal mechanism and depth for each event by minimizing the misfit between observed and synthetic *P/SH*, *P/SV* and *SH/SV* amplitude ratios. The ambiguity in the sense of motion on the nodal planes, arising owing to the use of amplitude ratios, is resolved by examining *P* wave polarities from the 5 stations of our digital network as well as stations of the OVSICORI-UNA permanent network for the larger aftershocks. The grid search technique allows errors associated with all fault geometries to be compared to better assess the significance of the global minimum and to avoid local minima.

All solutions with errors <30% above the minimum value are selected for further consideration. For each event the pressure and tension axes of the acceptable solutions are contoured on a lower-hemisphere, equal-area projection to evaluate the variation in mechanisms within the group of possible solutions and their consistency with *P* wave first-motion polarities. Contours of pressure (P) and tension (T) axes for the best focal mechanism solutions for six different aftershocks are shown in Figure 7. In some cases, such as for the events at 2323 UTC on May 10, 0316 UTC on May 12 and 1448 UTC on May 17 (Figure 7), the *P* and *T* axes for all potential solutions cluster, and the best solution is chosen as the mechanism with the lowest error that best fits the *P* wave first-motion polarities. For other events, two clusters of *P* and *T* axes are common (e.g., events at 1218 UTC on May 11, 1147 UTC on May 14 and 0214 UTC on May 18; see Figure 7), and the best solution is chosen as the mechanism with the smallest error that best fits the first motions and is most consistent with focal mechanisms from neighboring events. For most events where two clusters of *P* and *T* axes exist only one of these clusters is consistent with the first-motion data and the other cluster is rejected.

Our best focal mechanism solutions for 20 of the Costa Rica aftershocks are shown in Figure 8 and listed in Table 2. *Fan et al.* [1993] used waveforms recorded on the three midperiod sensors (stations CDMR, ZENR, and PANR) to determine focal mechanisms for 15 of the largest Costa Rica aftershocks employing a linear moment tensor inversion technique. Since *Fan et al.* [1993] used data from only midperiod stations and we required data to be available from the two short-period stations as well, our studies have only six events in common. Focal mechanism comparisons for these events are shown in Figure 9. In general, focal mechanism solutions obtained from waveform inversion (Figure 9, right) compare very well with those we determined using body wave amplitude ratios (Figure 9, left). The two fault plane solutions computed for the event on May 14 at 1115 UTC differ markedly from one another and provide the exception to this general agreement. *Fan et al.*'s [1993] moment tensor solution for this event has a large percent (37%) compensated linear vector dipole (CLVD), which may indicate a poorly determined solution. Their mechanism also violates several first motions (Figure 9). Synthetic seismograms computed for the midperiod stations CDMR and ZENR using the two different focal mechanism solutions fit the data poorly. However, the pure thrust mechanism of *Fan et al.* [1993] predicts *SH/SV* amplitude ratios that are much larger than observed at both stations. Observed *SH/SV* ratios close to 1 at station CDMR and 0.5 at ZENR are nearly matched with our oblique thrust mechanism.

Fan et al. [1993] calculated source-receiver distances and azimuths using different earthquake locations [*Schwartz and Protti*, 1991] from those reported here. The average difference in epicentral distance and depth for the six events for which we both determined focal mechanisms is 6.4 and 3.7 km, respectively. The generally favorable agreement between focal mechanisms computed with different techniques and with variations in hypocentral parameters similar or larger than our

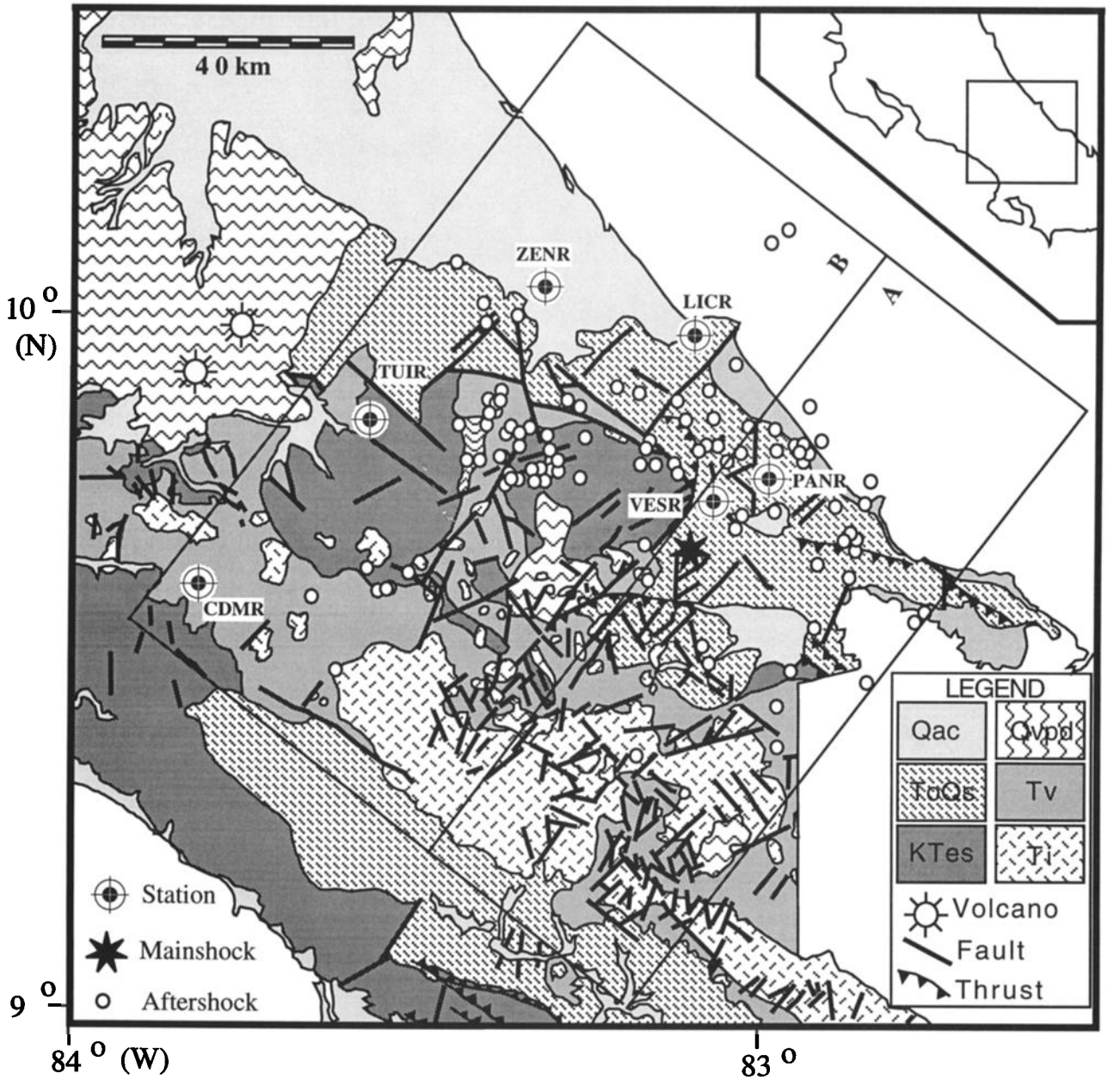

Figure 6. Aftershocks of the April 22, 1991, earthquake (circles) superimposed on a geologic map of southeastern Costa Rica modified from *Dondoli et al.* [1968] and *Ludington et al.* [1987]. Lithologic units are described in the text. Aftershocks located in boxes A and B are shown in schematic and interpretative cross sections in Figure 10. Inset shows location of larger map.

estimated location errors provides confidence that our fault plane solutions are not strongly affected by our average-estimated uncertainties in earthquake location. Hypocentral depth differences considerably larger than our average estimated uncertainty (~4 km) may result in different fault plane solutions. Three of the 20 events for which we computed fault plane solutions yielded depth mislocation errors >6 km in our synthetic simulation. Two of these events (0316 UTC on May 12 and 0735 UTC on May 14) produced considerably different fault plane solutions when the inversion was performed using two different crustal velocity models and hypocentral depths that differed by 6.5 and 9.9 km, respectively. Because our fault plane solutions are sensitive to relatively large errors in hypocentral parameters, which may exist for a few events in our data set, we make tectonic interpretations drawn from evaluation of a large number of events and do not over interpret any one single solution.

Results and Discussion

Tectonic Interpretation of Aftershock Locations and Focal Mechanisms

Examination of our focal mechanism solutions (Figures 8 and 10) and those determined by *Fan et al.* [1993] reveals a

Table 1. Earthquake Parameters

Origin Time		Latitude, N	Longitude, W	Depth, km	Magnitude, M_d	RMS, s	Reference
Date	Time, UTC						
May 9, 1991	2016:51.53	9°50.27'	83°23.81'	17.1	2.6	0.06	
May 10, 1991	0247:52.42	9°52.39'	83°23.45'	15.8	2.9	0.15	
May 10, 1991	0306:12.31	9°40.50'	82°51.78'	12.6	3.2	0.05	
May 10, 1991	0506:42.28	9°51.53'	83°22.95'	20.1	2.7	0.13	
May 10, 1991	1437:05.54	9°32.55'	82°54.81'	6.9	2.7	0.20	
May 10, 1991	1549:21.30	9°44.75'	83°21.45'	11.7	2.8	0.08	
May 10, 1991	1555:59.28	9°52.83'	83°10.34'	17.1	2.8	0.09	
May 10, 1991	1658:48.95	9°53.47'	83°12.33'	24.6	2.7	0.09	
May 10, 1991	2019:43.87	9°46.97'	83°17.40'	14.4	2.9	0.11	PS
May 10, 1991	2031:05.15	9°48.60'	82°54.47'	13.4	2.8	0.11	
May 10, 1991	2244:59.69	9°48.01'	83°03.47'	14.9	2.2	0.07	
May 10, 1991	2323:39.71	9°48.70'	83°20.26'	17.2	2.7	0.06	PS
May 11, 1991	0307:48.80	9°49.88'	83°21.97'	15.5	2.5	0.10	
May 11, 1991	0339:02.51	9°47.49'	83°10.26'	16.8	3.5	0.02	PS-FBW
May 11, 1991	0709:17.83	9°47.51'	83°22.45'	10.8	2.4	0.07	
May 11, 1991	0831:51.41	9°45.68'	83°20.43'	15.4	2.5	0.07	
May 11, 1991	0920:34.57	9°47.86'	82°56.09'	14.0	2.7	0.04	
May 11, 1991	0949:25.13	9°33.90'	82°45.28'	12.4		0.16	
May 11, 1991	1143:21.40	9°35.84'	83°33.35'	5.0	2.7	0.16	
May 11, 1991	1206:02.51	9°46.07'	83°17.21'	14.0	3.2	0.07	
May 11, 1991	1211:36.54	9°45.94'	83°18.28'	11.8	2.6	0.08	
May 11, 1991	1218:14.27	9°53.02'	83°22.40'	18.0	3.2	0.07	PS
May 11, 1991	1236:12.94	9°49.72'	82°58.50'	15.5	3.3	0.09	
May 11, 1991	1516:48.21	9°47.43'	83°22.17'	13.6	2.5	0.09	
May 11, 1991	1531:45.59	9°28.98'	82°57.01'	13.6	2.7	0.14	
May 11, 1991	1726:02.56	9°27.99'	82°49.96'	20.8	4.4	0.04	PS-FBW
May 11, 1991	1900:59.01	9°49.52'	83°20.17'	14.6	2.1	0.07	
May 11, 1991	2019:51.25	9°51.72'	83°15.38'	17.3	2.4	0.09	
May 12, 1991	0316:44.53	9°25.80'	82°58.14'	21.7	3.7	0.08	PS
May 12, 1991	0406:23.72	9°49.96'	83°21.90'	15.8	2.7	0.12	
May 12, 1991	0455:32.27	9°48.96'	83°20.96'	18.2	2.3	0.09	
May 12, 1991	0533:29.34	9°49.26'	83°18.50'	17.0	2.8	0.06	
May 12, 1991	0542:37.75	9°42.49'	82°58.54'	13.0	3.6	0.09	
May 12, 1991	0615:40.24	9°46.32'	83°19.58'	12.5	2.7	0.05	
May 12, 1991	1208:16.31	9°45.77'	83°06.97'	12.5	2.1	0.08	
May 12, 1991	1239:45.24	9°45.66'	83°21.83'	16.1	3.3	0.13	PS-FBW
May 12, 1991	1502:18.67	9°46.72'	83°07.12'	14.5	2.7	0.07	
May 12, 1991	1548:39.05	10°06.86'	82°57.36'	10.7	3.7	0.11	FBW
May 12, 1991	1623:35.92	10°05.80'	82°58.83'	11.8	2.5	0.20	
May 12, 1991	2201:29.03	9°29.67'	83°04.03'	16.2	2.9	0.07	
May 12, 1991	2203:31.33	9°52.03'	82°55.63'	18.2	3.0	0.16	PS
May 12, 1991	2247:02.09	9°47.09'	82°55.80'	14.7	3.9	0.05	FBW
May 12, 1991	2251:14.14	9°48.31'	82°56.50'	14.4	2.9	0.05	
May 12, 1991	2252:56.43	9°35.30'	83°39.12'	0.2	3.2	0.09	
May 13, 1991	0220:28.32	9°48.44'	83°18.32'	5.0	3.3	0.12	PS-FBW
May 13, 1991	0246:31.21	9°47.89'	83°01.27'	21.2	2.6	0.11	
May 13, 1991	0331:23.41	9°52.11'	83°22.56'	17.7	2.6	0.08	
May 13, 1991	0337:55.93	9°45.30'	82°49.93'	14.5	3.4	0.11	PS
May 13, 1991	0446:34.42	9°36.70'	83°09.77'	5.1	2.3	0.16	
May 13, 1991	0451:45.09	9°47.14'	83°24.27'	11.4	2.8	0.07	
May 13, 1991	0612:34.58	9°49.95'	83°00.75'	16.0	2.8	0.09	
May 13, 1991	0647:28.25	9°50.18'	83°26.17'	11.7		0.10	
May 13, 1991	0648:41.86	9°47.75'	82°55.41'	17.5	3.1	0.07	
May 13, 1991	0651:11.57	9°48.24'	82°55.86'	16.9	3.4	0.06	PS
May 13, 1991	0728:11.05	9°40.13'	82°51.04'	13.6	2.7	0.06	
May 13, 1991	0812:18.20	9°49.43'	83°22.18'	15.3	2.7	0.10	
May 13, 1991	0822:09.14	9°44.63'	83°02.74'	14.6	2.5	0.11	
May 13, 1991	1015:38.53	9°37.74'	83°30.66'	4.3	2.6	0.05	

Table 1. (continued)

Origin Time		Latitude, N	Longitude, W	Depth, km	Magnitude, M_d	RMS, s	Reference
Date	Time, UTC						
May 13, 1991	1019:07.34	9°47.80'	82°58.22'	13.3	3.1	0.10	PS
May 13, 1991	1027:59.57	9°48.14'	83°09.68'	20.7	2.9	0.11	
May 13, 1991	1039:50.86	9°46.60'	83°09.02'	20.4	2.9	0.11	
May 13, 1991	1254:09.03	9°48.82'	83°09.14'	20.5	2.7	0.06	
May 13, 1991	1412:32.04	9°48.13'	83°04.69'	17.7	2.9	0.06	
May 13, 1991	1542:21.02	9°45.31'	83°21.28'	18.0	2.9	0.11	
May 13, 1991	1602:14.13	9°48.07'	83°20.69'	13.9	2.4	0.05	
May 13, 1991	1735:54.65	9°21.70'	83°10.40'	7.9	2.4	0.93	
May 14, 1991	0619:26.17	9°50.52'	83°06.20'	14.4		0.09	
May 14, 1991	0716:38.52	9°48.32'	83°20.84'	16.7	2.6	0.06	
May 14, 1991	0735:53.94	9°55.31'	83°01.92'	19.2	2.5	0.07	PS
May 14, 1991	0804:21.66	9°51.09'	83°23.36'	18.8	2.5	0.06	
May 14, 1991	1115:48.45	9°42.21'	83°01.11'	13.9	3.7	0.09	PS-FBW
May 14, 1991	1147:03.94	9°38.06'	83°34.09'	12.7	3.1	0.08	PS
May 16, 1991	1912:31.07	9°59.70'	83°21.20'	14.9	2.3	0.11	
May 16, 1991	2025:12.38	10°00.73'	83°24.13'	17.1	2.6	0.11	
May 16, 1991	2139:36.58	9°43.31'	82°50.46'	13.6	3.3	0.06	
May 17, 1991	0122:34.83	9°51.32'	83°22.77'	16.0	3.8	0.12	PS-FBW
May 17, 1991	0138:47.36	9°36.90'	82°51.92'	13.0	3.7	0.03	FBW
May 17, 1991	0404:39.11	9°40.06'	83°09.68'	15.7	2.3	0.08	
May 17, 1991	1257:04.18	9°39.14'	82°51.54'	12.0	3.6	0.05	PS
May 17, 1991	1308:39.33	9°53.16'	83°04.46'	14.9	2.6	0.11	
May 17, 1991	1448:42.36	9°36.13'	83°32.57'	4.2	3.0	0.08	PS
May 17, 1991	2226:03.75	9°40.15'	82°52.40'	13.1	3.2	0.05	
May 18, 1991	0138:37.35	9°46.87'	83°02.70'	12.9	2.3	0.09	
May 18, 1991	0141:23.66	9°32.92'	82°46.05'	10.7		0.18	
May 18, 1991	0214:41.19	9°50.65'	83°03.87'	15.7	2.9	0.12	PS
May 18, 1991	0417:23.28	9°29.26'	83°36.89'	0.0		0.04	
May 18, 1991	0419:32.70	9°52.30'	83°16.58'	15.0	2.4	0.16	
May 18, 1991	0558:21.41	9°42.99'	82°53.15'	13.1	2.8	0.04	
May 18, 1991	0622:17.36	9°47.09'	83°18.00'	13.5	2.5	0.11	
May 18, 1991	0629:18.06	9°41.15'	83°01.95'	13.7	2.7	0.13	
May 18, 1991	1011:09.58	10°04.33'	83°26.49'	15.6	2.9	0.08	
May 18, 1991	1145:42.86	9°22.30'	82°58.13'	20.0	3.3	0.12	
May 18, 1991	1235:33.16	9°45.75'	83°21.14'	15.0	2.6	0.11	
May 18, 1991	1249:51.47	9°57.89'	83°05.98'	28.0	2.7	0.15	
May 18, 1991	1414:53.96	9°51.69'	83°22.89'	15.9	2.8	0.14	
May 18, 1991	1556:39.08	9°38.22'	82°54.70'	9.5	2.6	0.12	
May 18, 1991	1623:05.97	9°52.21'	83°07.15'	18.0	2.5	0.06	
May 18, 1991	2311:37.60	9°49.10'	83°15.09'	16.5	2.1	0.08	
May 19, 1991	0344:25.59	9°47.19'	83°25.41'	11.6	2.7	0.06	
May 19, 1991	0825:23.86	9°36.28'	83°32.23'	5.0	3.1	0.08	
May 19, 1991	0923:53.14	9°31.13'	83°04.95'	21.4	3.0	0.10	
May 19, 1991	1127:02.56	9°45.55'	83°18.31'	13.3	2.4	0.07	
May 19, 1991	1304:32.83	9°45.52'	83°15.43'	17.9	2.9	0.10	PS
May 19, 1991	1410:24.15	9°59.29'	83°23.96'	14.3	2.8	0.12	
May 19, 1991	1446:26.02	9°48.55'	83°04.35'	15.1	2.9	0.09	
May 19, 1991	2233:25.98	9°45.10'	83°19.15'	5.0	2.5	0.07	
May 20, 1991	0112:01.39	9°49.97'	83°19.95'	18.3	2.3	0.08	

PS indicates events with focal mechanisms determined in this study; FBW, events with focal mechanisms determined by *Fan et al.* [1993].

diversity of faulting geometries in the aftershock region of the April 22 Valle de la Estrella event, indicating a complex deformation of the aftershock volume. Thrust- and reverse-faulting solutions locate near the mainshock in the southeastern portion of the aftershock zone; normal faulting occurs northeast and northwest of the mainshock, and strike-slip solutions dominate along the western extension of the aftershock zone (Figure 8).

The aftershock distribution and focal mechanisms determined in this study, selected solutions from *Fan et al.*

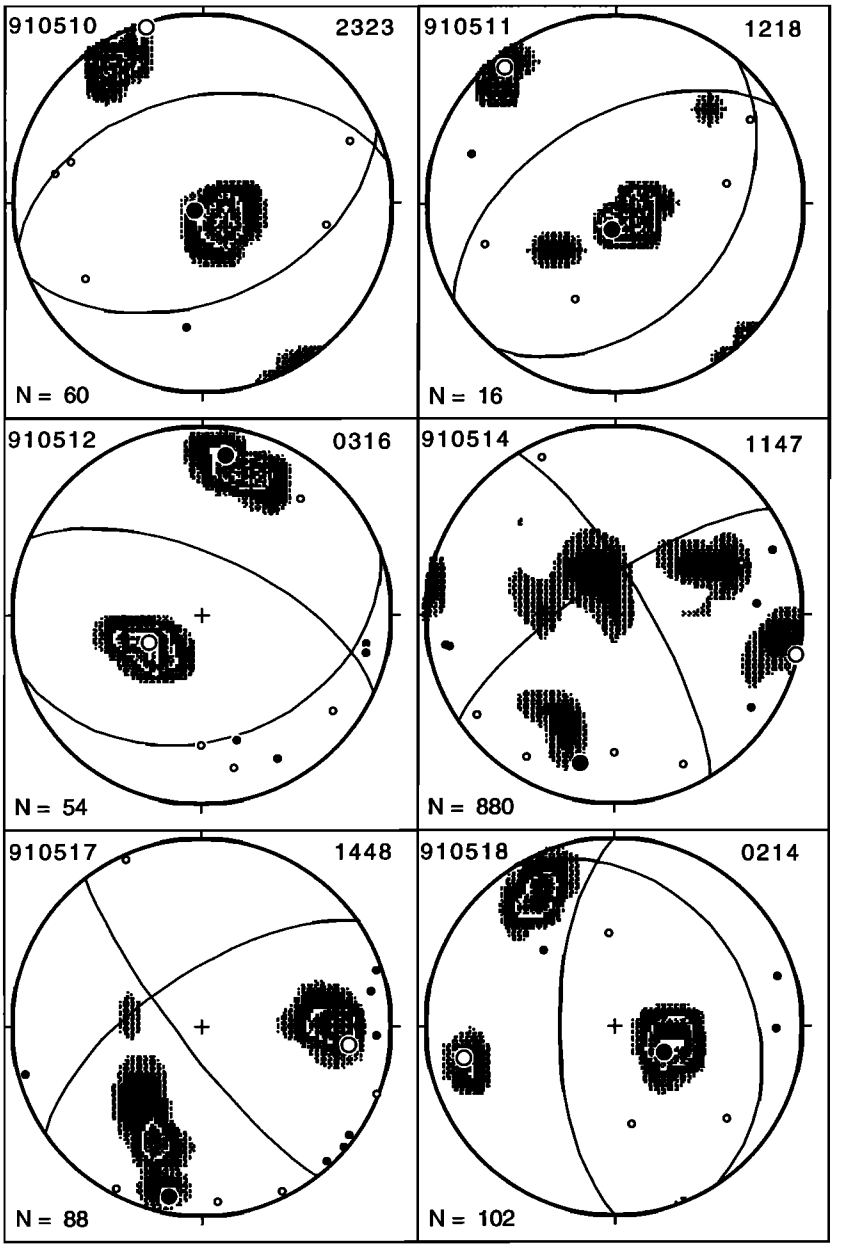

Figure 7. Contours of the density distribution of pressure and tension axes on equal-area, lower-hemisphere projections for all solutions having errors within 30% of the minimum for six aftershocks. Small solid and open circles represent compressional and dilatational first motions, respectively, from the temporary and permanent stations in Costa Rica. Large solid and open circles represent the *P* and *T* axes, respectively, corresponding to the best solution shown. *N* gives the number of *P* and *T* axes of acceptable solutions plotted.

[1993], and Harvard University centroid moment tensor solutions [*Dziewonski et al.*, 1991, 1992] are projected along SW-NE cross sections in Figure 10. We chose to display the focal mechanisms as side views projected onto the SW-NE sections so that the orientation of the nodal planes of each event can be compared directly with our faulting interpretations. Events in the southeastern portion of the aftershock zone (Figures 6, box A, and 10a) appear to define a horizontal thrust plane at a depth of ~15 km that we believe ruptured in the mainshock (Figure 10a). Although realistic error estimates in depth may be as large as ±4 km, the existence of a relatively horizontal distribution of earthquakes in this cross section is still distinguishable, especially when compared with the more clustered earthquake locations to the northwest (Figures 6, box B, and 10b). Focal mechanisms for many of the aftershocks that define the near-horizontal plane corroborate thrust motion on a near-horizontal plane. Our interpretation of cross section A is that the mainshock and many of the aftershocks occurred on this horizontal thrust and along imbricate faults associated with the basal decollément.

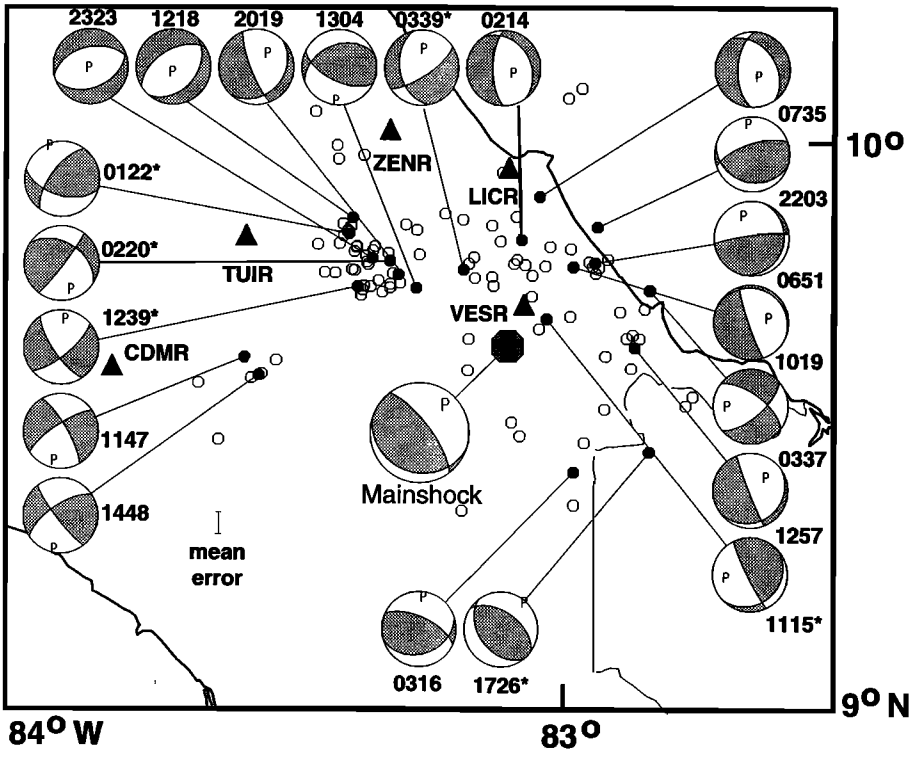

Figure 8. Mainshock and aftershock locations and lower-hemisphere, equal-area, focal mechanisms determined in this study. Shaded regions represent compressional quadrants. Events with asterisks also have mechanisms determined by *Fan et al.* [1993] which are compared with our solutions in Figure 9. Station locations are shown with triangles.

Intense folding and faulting mapped in this region [*Dondoli et al.*, 1968; *Ludington et al.*, 1987] indicate that many of these imbricate faults extend to the surface, but the absence of shallow depth aftershocks suggests that near-surface deformation occurs aseismically.

The sparse distribution of reverse faulting focal mechanisms, the abundance of aftershocks with strike-slip and normal faulting mechanisms, and the clustering of several aftershocks east of station TUIR (Figures 6 and 8) all suggest an important change in faulting geometry in the west portion of the aftershock zone (Figure 10b). The basal thrust imaged in the southeast (Figure 10a) is not evident to the northwest, and we believe that it transforms into several steep-dipping reverse faults that gradually become a NE-SW trending, elongated zone of left-lateral strike-slip faults. This rather diffuse zone of left-lateral strike-slip faults corresponds with the maximum northwest extension of this earthquake sequence and the NW boundary between the Panama block and the Caribbean plate. Figure 11 shows this interpretation schematically. Figure 11 integrates the main geological and tectonic features of the region with results of this study to clarify the interactions between the Caribbean plate and the Panama block in this developing convergent margin. The change in the fault geometry from southeast to northwest is represented by the steeping of the basal thrust from subhorizontal (SE part of the block diagram), to steeper NE-SW trending reverse faults in the northeast, to mainly left-lateral strike-slip faults in the northwest. This zone of strike-slip faults continues inland and appears to become part of the incipient, diffuse left-lateral transcurrent plate boundary between the Panama block and Caribbean plate across central Costa Rica, suggested by several authors [*Ponce and Case*, 1987; *Jacob and Pacheco*, 1991; *Güendel and Pacheco*, 1992;

Table 2. Focal Mechanism Parameters

Origin Time		Depth, km	Magnitude, M_d	Focal Mechanism		
Date	Time, UTC			Strike	Dip	Rake
May 10, 1991	2019	14.4	2.9	43	27	-28
May 10, 1991	2323	17.2	2.7	68	43	-96
May 11, 1991	0339	16.8	3.5	56	72	-53
May 11, 1991	1218	18.0	3.2	41	38	-104
May 11, 1991	1726	20.8	4.4	142	40	104
May 12, 1991	0316	21.7	3.7	72	34	53
May 12, 1991	1239	16.1	3.3	50	72	-18
May 12, 1991	2203	18.2	3.0	105	26	121
May 13, 1991	0220	05.0	3.3	37	85	46
May 13, 1991	0337	14.5	3.4	49	66	-151
May 13, 1991	0651	16.9	3.4	15	15	24
May 13, 1991	1019	13.3	3.1	161	84	-83
May 14, 1991	0735	19.2	2.5	182	57	-67
May 14, 1991	1115	13.9	3.7	47	21	162
May 14, 1991	1147	12.7	3.1	236	75	-14
May 17, 1991	0122	16.0	3.8	106	54	148
May 17, 1991	1257	12.0	3.6	56	17	-13
May 17, 1991	1448	04.2	3.0	236	67	10
May 18, 1991	0214	15.7	2.9	180	66	-74
May 19, 1991	1304	17.9	2.9	115	60	118

Strike, dip, and rake are in degrees.

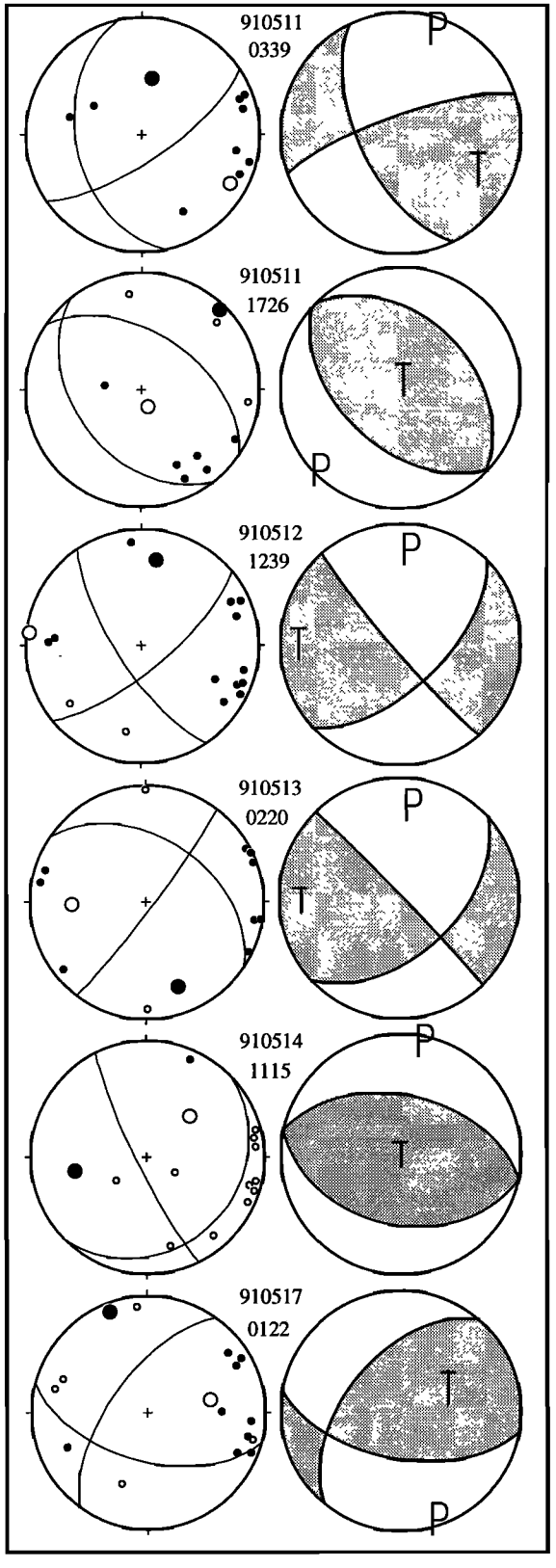

Figure 9. Comparison of (left) our focal mechanism solutions with (right) solutions by *Fan et. al.* [1993] for six aftershocks we have in common. Local, first-motion polarities and *P* and *T* axes are shown as in Figure 7.

Goes et al., 1993; *Fan et al.*, 1993; *Marshall et al.*, 1993]. The distribution of early aftershocks [*Montero et al.*, 1991] and the vertical deformation pattern [*Plafker and Ward*, 1992; *De Obaldía et al.*, 1991] favor this abrupt NW termination of the deformation volume associated with the 1991 Valle de la Estrella mainshock.

Geologic Control on Aftershock Location

The epicentral region of the April 22, 1991, earthquake is located within the southern part of the Limón basin of Costa Rica and the northern part of the Bocas del Toro basin of Panama. These two basins make up the largest sedimentary basin in southern Central America and contain an incomplete section of predominantly marine clastic deposits, Late Cretaceous to Quaternary in age, that exceed 7000 m in thickness [*Escalante*, 1990]. At the border between Costa Rica and Panama the basin is <50 km wide and is primarily located off-shore [*Escalante*, 1990; *Silver et al.*, 1990]. Following the geologic maps of *Dondoli et al.* [1968] and *Ludington et al.* [1987], we have divided the southern Limón Basin into two main lithological units (Figure 6). The lower unit (KTes) consists of competent Late Cretaceous to Eocene volcanic and volcaniclastic rocks interbedded with carbonate rocks [*Escalante*, 1990]. The upper, less competent unit (ToQs) is Oligocene to Pleistocene in age and consists of up to 7 km of fine grain, deep to shallow marine deposits overlain by coarse continental conglomerates [*Escalante*, 1990; *Astorga et al.*, 1991]. At the base of the upper unit is a 1000- to 3000-m sequence of soft argillaceous sandstones, shales, and claystones (Senosri formation) and soft fissile and monotonous sequence of shales (Uscari formation) [*Escalante*, 1990], representing an abrupt rheological contrast with the immediate underlying unit. West of the Limón Basin is the Talamanca Cordillera, a Miocene batholith (Ti) of intermediate composition. The lower unit of the Limón Basin as well as Late Tertiary volcanic rocks (Tv) outcrop on the northeastern flank of this cordillera (Figure 6).

The 260 located aftershocks of the April 22, 1991, earthquake are confined to depths from 0 to 28 km. While deeper events are widely distributed, shallow events are restricted to areas where the lower unit of the basin or the Miocene batholith outcrops and particularly near the mapped contacts with the overlying unit (Figures 6, 8, and 10 show only the best 107 aftershock locations). It is important to note here that all mapped geological contacts between these two units are by faulting [*Dondoli et al.*, 1968; *Ludington et al.*, 1987] (Figure 6). No earthquakes locate within the strongly folded upper unit. We believe that the rheological properties of these deposits inhibit the upward transfer of brittle slip from the more competent lower unit. Rather than fail brittlely, the upper basin unit deforms plastically, generating folds. Detachment through aseismic axial faulting can also represent a fraction of that slip transfer. Mapped thrust faults [*Dondoli et al.*, 1968; *Ludington et al.*, 1987] and offshore reflection profiles [*Astorga et al.*, 1991; *Silver et al.*, 1990] show SW dipping thrust faults within the upper unit, consistent with the faulting associated with the mainshock (Figure 10).

The steep gradient from NW to SE, in coastal vertical deformation associated with the mainshock [*Plafker and Ward*,

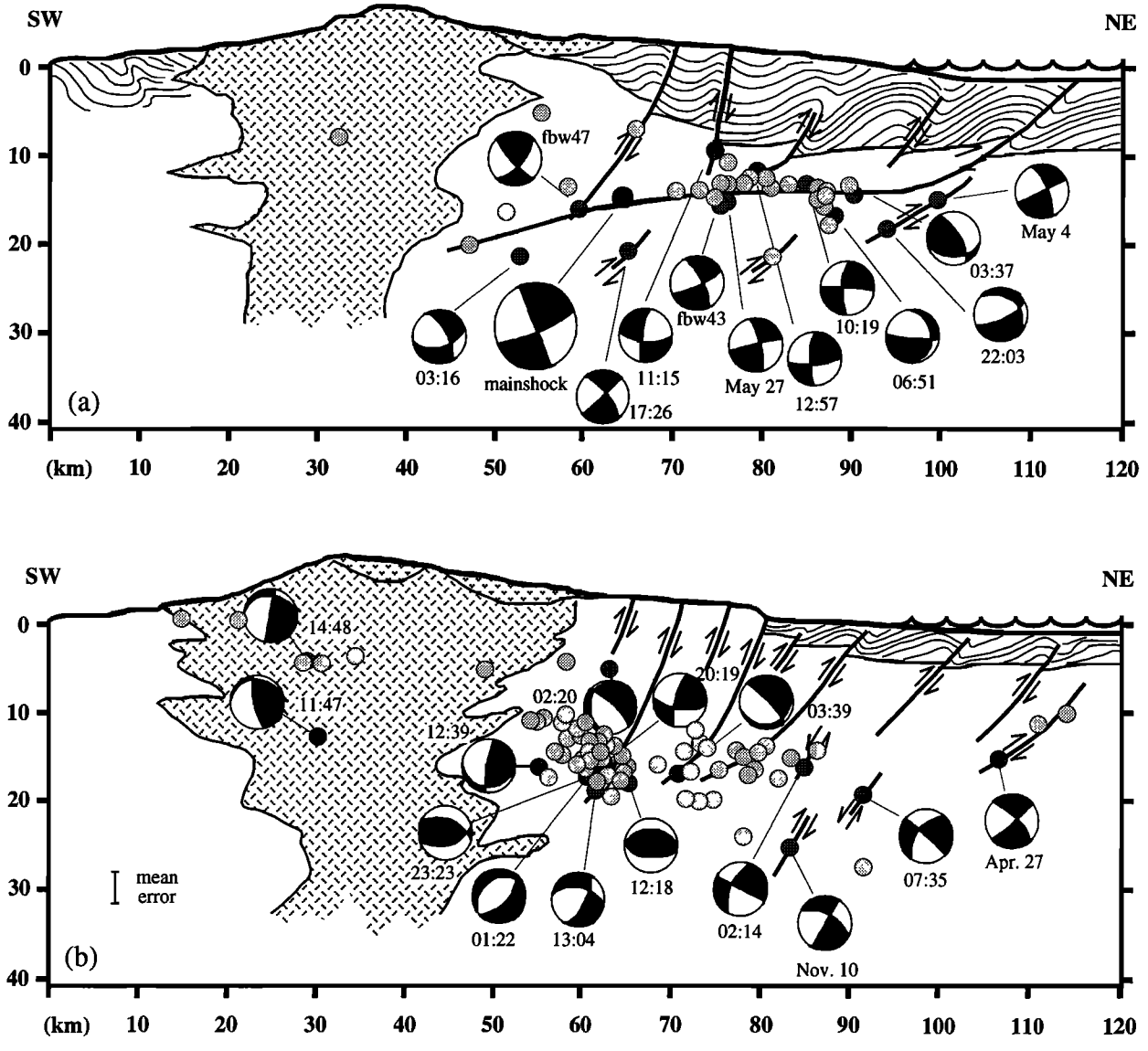

Figure 10. Schematic and interpretative geologic cross sections through the aftershock zone of the April 22, 1991, Costa Rica event for aftershocks in (a) Figure 6, box A and (b) Figure 6, box B. Side view focal mechanisms determined in this study (hour:minute), by *Fan et al.* [1993] (fbw number) and Harvard University centroid moment tensor solutions (month day) have been projected onto the cross section. For legend, see Figure 6.

1992; *De Obaldía et al.*, 1991], could also be the effect of the local geology. Under Limón, where the maximum uplift occurred, the lower unit is very shallow, so seismic or brittle slip could propagate close to the surface, producing a large amount of vertical uplift. To the southeast the existence of a thick upper unit may have caused the slip to terminate at deeper depth, resulting in a smaller vertical uplift and perhaps folding of the sedimentary package. The absence of mainshock and aftershock slip near the surface suggests that the April 22, 1991, earthquake is a blind thrust event.

Valle de la Estrella and Other Blind Thrust and Back Arc Earthquakes

Blind thrust earthquakes, in addition to not rupturing the surface, are characterized by their occurrence beneath folded sedimentary basins (buried thrust faulting is actually the mechanism for fold growth [*Stein and Yeats*, 1989]). In blind thrust events the mainshock nucleates on shallow dipping (12-25°) planes without surface expression and their aftershocks locate both along the mainshock [*Ekström et al.*, 1992] and fill a diffuse zone that occupies a region much larger than the site of coseismic slip [*Stein and Ekström*, 1992]. Classic examples of earthquakes occurring on blind thrust faults are the 1982 New Idria, 1983 Coalinga, 1985 Kettleman Hills [*Ekström et al.*, 1992; *Stein and Ekstrom*, 1992], 1987 Whittier Narrows [*Hauksson and Jones*, 1989], California, earthquakes and the 1985 Nahanni, Canada, earthquakes [*Wetmiller et al.*, 1988]. Most blind thrust earthquakes occur in continental environments.

The 1991 Valle de la Estrella earthquake shares several characteristics with blind thrust events. It occurred on a

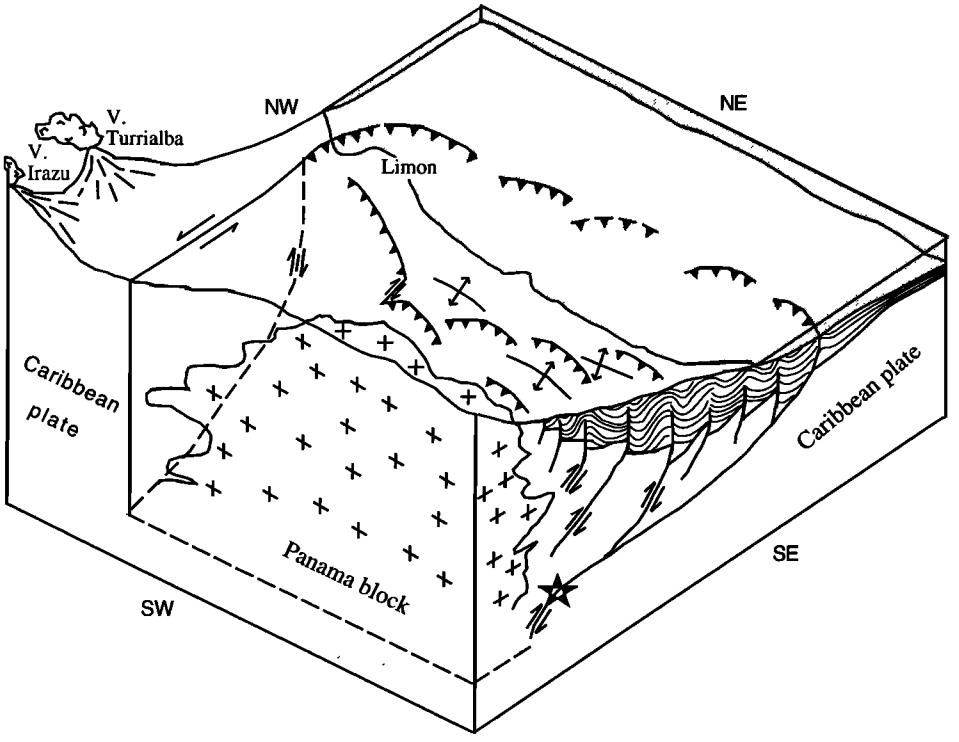

Figure 11. Schematic block diagram showing our interpretation of Costa Rica back arc deformation illuminated by the April 22, 1991, mainshock and aftershock sequence.

subhorizontal plane buried beneath a thick sedimentary basin and produced a diffuse pattern of aftershocks. The existence of mapped thrust faults (mainly fold related) in the epicentral area of the Costa Rica earthquake [*Dondoli et al.*, 1968; *Ludington et al.*, 1987] (Figure 6) makes this event myopic rather than totally blind. A rheological contrast similar to what exists in the Limón Basin also occurs in the region of the 1985 Nahanni, Canada, thrust earthquakes. There a fold belt exists with a thick package of shales at the base overlying a Precambrian crystalline basement [*Wetmiller et al.*, 1988]. Similar to our interpretation of coseismic slip abruptly terminating at the base of the less competent Senosri and Uscari formations during the Costa Rica earthquake, transfer of seismic slip from the crystalline basement to the surface also may have been inhibited by the overlying less competent section of shales during the Nahanni earthquakes. The existence of mapped thrust faults in the region of the Canadian events, as in the case of the Costa Rica earthquake, makes them myopic too.

Another interesting feature that the Valle de la Estrella earthquake has in common with other blind or myopic thrust earthquakes is the discrepancy between the dip of the fault plane obtained from local first-motions and teleseismic waveform inversions. For example, the shallow dipping nodal plane obtained from first motions for the 1985 Kettleman Hills earthquake is steeper than that obtained from waveform inversion at teleseismic distances [*Ekström et al.*, 1992]. For the Valle de la Estrella event, *Montero et al.* [1991] obtained a fault plane dipping 40° from local first motions, while *Goes et al.* [1993] obtained dips of 21±10° from surface waves and 15-20° from body waves. For the Costa Rica event we interpret this discrepancy as evidence for earthquake nucleation on a steeper fault (represented by the first-motion mechanism) at depth, with updip propagation along the subhorizontal basal thrust imaged in Figure 10a. This rupture scenario would result in an average, overall far-field dip that was shallower than the first-motion mechanism. Body and surface wave analysis [*Goes et al.*, 1993] as well as GPS data [*Lundgren et al.*, 1993] are consistent with updip rupture. *Ekström et al.* [1992] interpreted the focal mechanism discrepancy for the 1985 Kettleman Hills event as evidence for downdip rupture propagation from a steep-dipping fault to a shallow-dipping listric fault. We believe that in these cases the direction of rupture is controlled by the local geology. While in the Kettleman Hills region, competent rocks exist at shallow levels that may allow earthquake nucleation, in the Limón Basin the incompetent character of the sedimentary package inhibited nucleation of the Valle de la Estrella earthquake at shallow depths.

The 1964 Niigata, 1983 Akita-Oki, and 1993 Sea of Japan earthquakes and the 1978 and 1992 Flores earthquakes occurred in a similar back arc setting as the Valle de la Estrella earthquake. A deformation model for the Niigata earthquake [*Satake and Abe*, 1983] and inversion of long-period surface waves for the Akita-Oki earthquake [*Kanamori and Astiz*, 1985; *Satake*, 1985] indicate underthrusting of the Sea of Japan ocean floor beneath the active northern Japanese arc; body wave inversion and gravity data modeling for the 1978 Flores earthquake [*McCaffrey and Nábêlek*, 1984] and body and surface wave inversions for the 1992 Flores earthquake [*Beckers and Lay*, 1993] indicate underthrusting of the Banda Sea floor beneath the back arc of eastern Sunda. In both the

Sea of Japan and the Sunda arc, underthrusting of oceanic lithosphere beneath an active arc is similar to underthrusting of the Caribbean plate beneath the Panama block. All these back arc events may represent the manifestation of early stages in the formation of new subduction zones behind active convergent plate margins. *Goes et al.* [1993] compared the stress drop of the 1991 Costa Rica earthquake with that of the Niigata and Akita-Oki earthquakes and concluded that the stress drops for these three events are more consistent with stress drops characteristic of interplate events than intraplate events, supporting the idea that these regions are nascent plate boundaries.

Conclusions

The April 22, 1991, M_W=7.7 Valle de la Estrella, Costa Rica, earthquake represents back arc thrusting of the Caribbean plate beneath the Panama block along the North Panama Thrust Belt. We have located 107 aftershocks and obtained focal mechanism solutions for 20 of the larger, well-located events. We image the basal decollément at a depth of ~15 km in the southeast portion of the aftershock zone. Deeper aftershocks (10-28 km) are widely distributed; shallow ones are restricted to areas where the lower unit of the southern Limón basin outcrops and particularly near the mapped contacts with the overlying unit. This suggests that surface exposure of the lower unit results from repeated earthquake slip on the shallow crustal faults imaged by the aftershocks. No aftershocks locate within the strongly folded upper unit. We believe that rheological properties of these deposits inhibit the upward transfer of brittle slip from the more competent lower unit. The absence of both mainshock and aftershock slip near the surface suggests that the 1991 Valle de la Estrella earthquake is a blind thrust event. This event shares several characteristics with other blind thrust earthquakes, including its occurrence on a shallow-dipping plane beneath a folded sedimentary basin and its diffuse aftershock zone.

A diffuse zone of left-lateral strike-slip faults marks the northwest terminus of the 1991 Valle de la Estrella earthquake rupture volume and represents part of the western boundary of the Panama block with the Caribbean plate. Our work contributes more evidence for a young diffuse plate boundary between the Panama block and the Caribbean plate across Costa Rica.

Acknowledgments. We would like to thank IGPP at the University of California at San Diego and at Lawrence Livermore National Laboratory for providing the instruments used in the portable deployment. Susan Beck, Karen McNally, Walter Schillinger, Gerry Simila, Aaron Velasco, and George Zandt were part of the U.S. team. Deployment of the digital network would not have been possible without the institutional and logistical support from the Costa Rica Volcanological and Seismological Observatory; we particularly thank Eduardo Malavassi, Victor González, Henri Rodríguez, Carlos Montero, and Daniel Rojas; Oscar Barrantes provided the arrival times and coda durations for station LICR. We also thank Javier Pacheco, Fumiko Tajima, and an anonymous reviewer for their suggestions that improved this manuscript. This research was supported by NSF grant EAR-9018487 (S. Y. Schwartz). NSF grant EAR-9115667 to K. McNally provided financial support for the field instrument deployment. Facilities support was provided by the W. M. Keck Foundation. This is contribution 228 of the Institute of Tectonics and contribution 169 of the Observatorio Vulcanológico y Sismológico de Costa Rica.

References

Astorga, A., J. A. Fernández, G. Barboza, L. Campos, J. Obando, A. Aguilar, and L. G. Obando, Cuencas sedimentarias de Costa Rica: Evolución geoquímica y potencial de hidrocarburos, *Rev. Geol. Am. Cent., 43*, 25-59, 1991.

Beckers, J., and T. Lay, Rupture process of the Tsunamigenic December 12, 1992 Flores, Indonesia Earthquake (Mw=7.7) (abstract), *Eos, Trans. AGU 74*(43) Fall Meeting suppl., 398, 1993.

DeMets, C., R. G. Gordon, D. F. Argus, and S. Stein, Current plate motions, *Geophys. J. Int., 101*, 425-478, 1990.

De Obaldía, F., T. Marino, R. Van Der Laat, F. Hernández, E. Malavassi, and K. McNally, Coseismic uplift associated with the Costa Rica earthquake (Ms 7.5) of April 22, 1991 (abstract), *Eos Trans. AGU 72*(44) Fall Meeting suppl., 301,1991.

Dondoli, C., G. Dengo, and E. Malavassi, Mapa geológico de Costa Rica, scale 1:700, 000, Inst. Geogr. Nac., San José, Costa Rica, 1968.

Dziewonski, A. M., G. Ekström, and M. P. Salganik, Centroid-moment tensor solutions for April-June, 1991, *Phys. Earth Planet. Inter., 71*, 6-14, 1991.

Dziewonski, A. M., G. Ekström, and M. P. Salganik, Centroid-moment tensor solutions for October-December, 1991, *Phys. Earth Planet. Inter., 74*, 89-100, 1992.

Ekström, G., R. S. Stein, J. P. Eaton, and D. Eberhart-Phillips, Seismicity and geometry of a 110-km-long blind thrust fault, 1., The 1985 Kettleman Hills, California, earthquake, *J. Geophys. Res., 97*, 4843-4864, 1992.

Escalante, G., Geology of southern Central America and western Colombia, in The Caribbean Region, *The Geology of North America*, edited by G. Dengo and J.E. Case, pp. 201-230, Geological Society of America, Boulder, Colo. 1990.

Fan, G. W., S. L. Beck, and T. C. Wallace, The seismic source parameters of the 1991 Costa Rica aftershock sequence: Evidence for a transcurrent plate boundary, *J. Geophys. Res., 98*, 15,759-15,778, 1993.

Goes, S. D. B., A. A. Velasco, S. Schwartz, and T. Lay, The April 22, 1991, Valle de la Estrella, Costa Rica (Mw=7.7) earthquake and its tectonic implications: A broadband seismic study, *J. Geophys. Res., 98*, 8127-8142, 1993.

Güendel, F., Seismotectonics of Costa Rica: An analytical view of the southern terminus of the Middle American Trench, Ph.D. dissertation, Univ. of Calif., Santa Cruz, 1986.

Güendel, F., and J. Pacheco, The 1990-1991 seismic sequence across central Costa Rica: Evidence for the existence of a micro-plate boundary connecting the Panama deformed belt and the Middle America trench, (abstract), *Eos Trans. AGU, 73*(43), Fall Meeting suppl., 399, 1992.

Güendel, F., et al., Mainshock-aftershock sequence associated with the Costa Rica earthquake (*Ms*=7.5) of April 22, 1991 (abstract), *Eos Trans. AGU, 72*(44), Fall Meeting suppl., 300, 1991.

Hauksson, E., and L. M. Jones, The 1987 Whittier Narrows earthquake sequence in Los Angeles, southern California: Seismological and tectonic analysis, *J. Geophys. Res., 94*, 9569-9589, 1989.

Jacob, K. H., and J. Pacheco, The M-7.4 Costa Rica earthquake of April 22, 1991: Tectonic setting, teleseismic data, and consequences for seismic hazard assessment, *Earthquake Spectra, 7*, suppl. B, 15-33, 1991.

Kanamori, H., and L. Astiz, The 1983 Akita-Oki earthquake (Mw=7.8) and its implications for systematics of subduction earthquakes, *Earthquake Predict. Res., 3*, 305-317, 1985.

Kisslinger, C., Evaluation of S to P amplitude ratios for determining focal mechanisms from regional network observations, *Bull. Seismol. Soc. Am., 70*, 999-1014, 1980.

Ludington, S., R. Castillo, and H. Azuola, Geology of Costa Rica, in mineral resources assessment of the Republic of Costa Rica, *U.S. Geol. Surv. Misc. Invest. Map I-1865*, 6-7, 1987.

Lundgren, P., S. K. Wolf, M. Protti, and K. J. Hurst, GPS measurements

of crustal deformation following the 22 April 1991, Valle de la Estrella, Costa Rica, earthquake, *Geophys. Res. Lett., 20*, 407-410, 1993.

Marshall, J. S., D. M. Fisher, and T. W. Gardner, Western margin of the Panama microplate, Costa Rica: Kinematics of faulting along a diffuse plate boundary, *Geol. Soc. Am. Abstr. Programs, 25*(6), A-284, 1993.

Matumoto, T., M. Othake, G. Latham, and J. Umaña, Crustal structure of southern Central America, *Bull. Seismol. Soc. Am., 67*, 121-134, 1977.

McCaffrey, R., and J. Nábêlek, The geometry of back arc thrusting along the eastern Sunda Arc, Indonesia: Constraints from earthquake and gravity data, *J. Geophys. Res., 89*, 6171-6179, 1984.

Montero, C., et al., Observaciones iniciales obtenidas luego del terremoto del 22 de Abril de 1991, Ms=7.4, Valle de la Estrella, Costa Rica, informe preliminar, 27 pp., Obs. Vulcanol. y Sismol. de Costa Rica, Univ. Nac., Heredia, Costa Rica, 1991.

Nelson, G., and J. Vidale, Earthquake locations by 3-D finite-difference travel times, *Bull. Seismol. Soc. Am., 80*, 395-410, 1990.

Pearce, R. G., The relative amplitude method applied to 19 March 1984 Uzbekistan earthquake and its aftershocks, *Phys. Earth Planet. Inter., 47*, 137-149, 1987.

Plafker, G., and S. N. Ward, Back arc thrust faulting and tectonic uplift along the Caribbean Sea coast during the April 22, 1991, Costa Rica earthquake, *Tectonics, 11*, 709-718, 1992.

Ponce, D. A., and J. E. Case, Geophysical interpretation of Costa Rica, in Mineral resources assessment of the Republic of Costa Rica, *U.S. Geol. Surv. Misc. Invest. Map, I-1865*, 8-17, 1987.

Protti Quesada, M., V. González, and F. Güendel, *Earthquake Catalog 1986*, 151 pp., Observatorio Vulcanológico y Sismológico de Costa Rica, Universidad Nacional, Heredia, Costa Rica, 1987.

Rognvaldsson, S., and R. Slunga, Routine fault plane solutions for local networks: A test with synthetic data, *Bull. Seismol. Soc. Am., 83*, 1232-1247, 1993.

Satake, K., The mechanism of the 1983 Japan Sea earthquake as inferred from long-period surface waves and tsunamis, *Phys. Earth Planet. Inter., 37*, 249-260, 1985.

Satake, K., and K. Abe, A fault model for the Niigata, Japan, earthquake of June 16, 1964, *J. Phys. Earth, 31*, 217-223, 1983.

Schwartz, S., Source parameters of local earthquakes from inversion of P and S wave amplitudes (abstract), *Eos Trans. AGU 74*(43), Fall Meeting suppl., 399, 1993.

Schwartz, S., and M. Protti, Aftershock locations of the April 22, 1991 Valle de la Estrella, Costa Rica earthquake from portable digital stations (abstract), *Eos Trans. AGU 72*(44), Fall Meeting suppl. 302, 1991.

Schwartz, S., et al., A portable aftershock deployment in the region of the April 22, 1991 Valle de la Estrella, Costa Rica earthquake (abstract), *Eos Trans. AGU 72*(44), Fall Meeting suppl. 302, 1991.

Silver, E. A., D. L. Reed, J. E. Tagudin, and D. J. Heil, Implications of the north and south Panama thrust belt for the origin of the Panama orocline, *Tectonics, 9*, 261-281, 1990.

Slunga, R., Earthquake source mechanism determination by use of body-wave amplitudes - An application to Swedish earthquakes, *Bull. Seismol. Soc. Am., 71*, 25-35, 1981.

Stein, R., and G. Ekström, Seismicity and geometry of a 110-km-long thrust fault, 2., Synthesis of the 1982-1985 California earthquake sequence, *J. Geophys. Res., 97*, 4865-4883, 1992.

Stein, R., and R. S. Yeats, Hidden earthquakes, *Sci. Am., 260* (6), 48-57, 1989.

Vidale, J., Finite-difference calculation of travel times in three-dimensions, *Geophysics, 55*, 521-526, 1990.

Wang, C. Y. , and R. B. Herrmann, A numerical study of P-, SV- and SH-wave generation in a plane layered medium, *Bull. Seismol. Soc. Am., 70*, 1015-1036, 1980.

Wetmiller, R. J., R. B. Horner, H. S. Hasegawa, R. G. North, M. Lamontagne, D.H. Weichert, and S.G. Evans, An analysis of the 1985 Nahanni earthquakes, *Bull. Seismol. Soc. Am., 78*, 590-616, 1988.

Zhao, D., A. Hasegawa, and S. Horiuchi, Tomographic imaging of P and S wave velocity structure beneath northeastern Japan, *J. Geophys. Res., 97*, 19,909-19,928, 1992.

M. Protti, Observatorio Vulcanológico y Sismológico de Costa Rica, Universidad Nacional, Heredia, Apartado 86-3000, Heredia, Costa Rica (e-mail: protti@earthsci.ucsc.edu)

S. Schwartz, Institute of Tectonics and Earth Sciences Department, University of California, Santa Cruz, CA 95064 (e-mail: susan@earthsci.ucsc.edu)

(Received December 27, 1993; revised May 9, 1994;
accepted May 18, 1994.)